Simulating the Gas Diffusion Coefficient in Macropore Network Images: Influence of Soil Pore Morphology

Gang Liu, Baoguo Li,* Kelin Hu, and M. Th. van Genuchten

ABSTRACT

Knowledge of the diffusion coefficient is necessary for modeling gas transport in soils and other porous media. This study was conducted to determine the relationship between the diffusion coefficient and pore structure parameters, such as the fractal dimension of pores (D_{mp}), the shortest path length through the medium (l_{min}), and the fractal dimension of the shortest path (D_{min}). The finite element method (FEM) was used to simulate the gaseous diffusion process in an idealized soil system with a highly connected macropore network. The analysis was performed on binary images of soil thin sections. We show that the ratio ξ of the diffusion coefficient in soil (D_{eff}) to that in free air (D_0) is a function of not only the air-filled porosity ε, but also of other parameters, and hence no universal relationship exists between ξ and D_{mp} and D_{min}. Furthermore, ξ is shown to be strongly related to the pore-space structure and the direction of the concentration gradient. The tortuosity (T) furthermore was found to be related to the weighted path length along the main diffusion direction.

When advective transport is minimal, diffusion will be the dominant transport process for gases in soils. Gaseous diffusion controls such phenomena as soil aeration (Buckingham, 1904; Taylor, 1949), fumigant emissions (Brown and Rolston, 1980), volatilization of volatile organic chemicals from contaminated sites (Petersen et al., 1996), and the sequestration or emission of greenhouse gases such as methane into or from soils (Kruse et al., 1996). Knowledge of diffusion is critical to developing accurate predictive models for gas flow in porous media, and to improving our understanding of the basic transport processes involved (e.g., Park et al., 2001).

Numerous models have been developed over the years for the relative diffusion coefficient ξ, defined as the ratio of the diffusion coefficient in soil (D_{eff}) to that in free air (D_0), as a function of soil type and the air-filled porosity, ε. Following Moldrup et al. (2004), these models may be divided into two groups. One group of models attempts to relate ξ to the total porosity, Φ, and the water content, θ. This group includes a linear model suggested by Penman (1940) and a nonlinear formulation by Marshall (1959) that contains ε as the only adjustable parameter. Empirical nonlinear models that contain both ε and Φ as adjustable parameters include the model of Millington and Quirk (1960)

$$\xi = \varepsilon^{10/3}/\Phi^2 \quad [1]$$

and the model of Millington and Quirk (1961)

$$\xi = \varepsilon^2/\Phi^{2/3} \quad [2]$$

Moldrup et al. (1999, 2001) later used the Campbell soil water retention exponent b as a third model parameter.

Another group of models for ξ is based on the pore-size distribution of soils (Arah and Ball, 1994; Steele and Nieber, 1994). Recently fractal theory has also been used to derive models of this type (Anderson et al., 2000). While these models have been found to perform well in terms of fitting individual data sets, they are based on the assumption that some unique relationship exists between ξ and ε. This assumption contradicts some experimental data, such as those from Bruckler et al. (1989) and Jin and Jury (1996) shown in Fig. 1. This figure contains experimental data of ξ, versus ε taken from several literature sources. The considerable variability in the data from Bruckler et al. (1989) has been attributed to differences in pore morphology between the various samples. Also, because of the phenomenological nature of the Millington and Quirk models, the physical meaning of the exponents in those models is unclear. The parameters ε, Φ, and D_{mp} in these models are unable to reflect the non-isotropic characteristic of a porous network, the distribution of pores, and the proportion of the porosity occupied by blind or dead-end pores. For these reasons it is difficult to use these models to predict ξ for a given structure with specific pore morphology.

As compared with the large number of models for ξ currently available, only two effective methods exist for simulating diffusion at the pore scale: the lattice-Boltzmann method (LBM) and the FEM. The LBM uses a grid made up of a number of lattice points that are connected with some of their neighbors by means of bonds. Alvarez-Ramirez et al. (1996), Martys (1999), and Weerts et al. (2001) demonstrated the advantages of LBM in simulating diffusion in porous media. Unfortunately, the LBM is usually applied to uniform, regular spatial lattices (Peng et al., 1998). This limitation is too severe for complex soil pore geometries that cannot be fitted easily with a regular (structured) lattice.

The FEM, by contrast, can be adapted more easily to problems with transport domains of complex geometry, especially if an unstructured mesh is used. The FEM is a method for solving partial differential equations by

G. Liu, B. Li, and K. Hu, Lab. for Plant-Soil Interaction Processes, Ministry of Education, College of Resources and Environment, China Agricultural Univ., No. 2 Yuanmingyuan Xi Lu, Beijing 100094, P.R. China; M.Th. van Genuchten, USDA-ARS, George E. Brown, Jr., Salinity Lab., 450 West Big Springs Rd., Riverside, CA 92507, USA. Received 24 June 2005. *Corresponding author (libg@cau.edu.cn).

Published in Soil Sci. Soc. Am. J. 70:1252–1261 (2006).
Soil Physics
doi:10.2136/sssaj2005.0199

677 S. Segoe Rd., Madison, WI 53711 USA

Abbreviations: 2D, two dimensional; 3D, three dimensional; BTC, breakthrough curve; FEM, finite element method; LBM, lattice–Boltzmann Method.

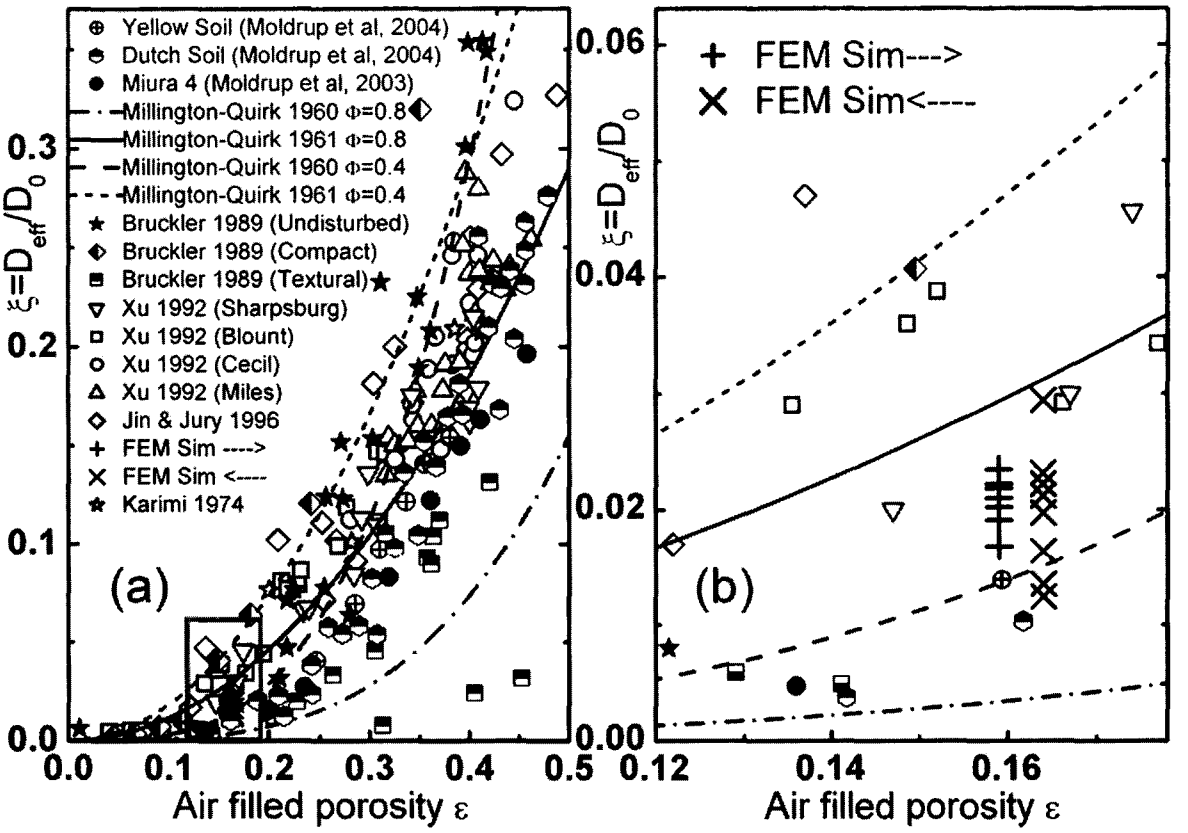

Fig. 1. (a) Comparison of measured and finite element (FEM) simulated value of ξ with the commonly used Milling-Quirk models. Data sources: Karimi et al. (1987); Jin and Jury (1996); Bruckler et al. (1989); Xu et al. (1992); and Moldrup et al. (2003, 2004). FEM results are marked by + (inlet at the left boundary) and × (inlet at the right boundary). (b) Enlarged area within gray lines of (a).

approximating continuous variables by a set of values in discrete points, located at a certain grid or mesh (Brenner and Scott, 1994). The FEM is a powerful tool for solving problems in structural analysis and fluid mechanics (Kimmich et al., 2001), for analysis of electromagnetic fields (Bolvin et al., 2004), and for solving complex subsurface flow and contaminant transport problems (e.g., Rassam et al., 2003). In this study we used the FEM to analyze pore-scale diffusion in two-dimensional (2D) soil thin sections. Two factors motivated us to use 2D soil thin sections in our FEM simulations. First of all, Anderson et al. (1996, 2000) and Weerts et al. (2001) previously performed extensive research on 2D soil thin sections, which were available to us in digitized 2D form rather than in the form of full three dimensional (3D) structures or 3D graphs. Second, the requirements for complete 3D FEM simulations of a porous medium are generally still beyond the capability of personal computers.

In this paper, we present the results of FEM simulations of diffusion in eight digitized 2D soil thin sections. We first examine the possible existence of a unique relationship between ξ and porosity (i.e., whether or not different diffusion coefficients can be associated with a certain porosity). Next we analyze the relationship between ξ and pore space morphology and soil structure, and search for alternative macroscopic parameters that may better describe the diffusion process.

THEORETICAL

Diffusion Equation

Quantitative descriptions of diffusion originated with studies by Graham (1850) and Fick (1855) some 150 yr ago. These authors conducted extensive diffusion experiments and noted that the amount of material transferred by diffusion was proportional to the concentration difference. Using analogies from the conduction of heat and electricity, Fick (1855) formulated what is now known as Fick's first law of diffusion:

$$j = -D_0 \nabla C \qquad [3]$$

where j (kg m^{-2} s^{-1}) is the mass flux per unit area, D_0 (m^2 s^{-1}) is the diffusion coefficient, C (kg m^{-3}) is the concentration. Combing Eq. [3] with the mass balance equation yields

$$\frac{\partial C}{\partial t} + \nabla \cdot j = 0 \qquad [4]$$

where t is time(s). When the diffusion coefficient is constant, Eq. [4] reduces to

$$\frac{\partial C}{\partial t} = D_0 \nabla^2 C \qquad [5]$$

Applicability of the Classical Diffusion Equation

Although Fick's law may not describe the motion of particles confined to a fractal or random structure, Eq. [3] is assumed to hold for the diffusion process in our simulated domains derived from soil thin sections. We rely on the fact that the dif-

fusion coefficient is related to microscopic parameters through $D = \lambda \langle v \rangle/3$, where $\langle v \rangle$ is the mean velocity of the gas and λ the mean free path length (Satoh et al., 1995). For air at 0.101 MPa (1 atm) and 0°C, $\lambda \approx 5 \times 10^{-8}$ m, and $\langle v \rangle = 488$ m s^{-1} (Satoh et al., 1995). The size of the smallest pores used in our simulation was approximately 10^{-4} m, which is at least 10^4 times larger than λ. Hence, Fick's law should provide a good approximation for diffusion in the idealized soil system used in this study.

Exact Solution of the Diffusion Equation

We make the following assumptions: (1) diffusion is the only dynamic process, while advection is negligible, (2) adsorption and desorption are negligible and (3) the diffusion macroscopically is one-dimensional. The general gas transport equation then reduces to the diffusion equation

$$\frac{\partial C(x,t)}{\partial t} = D_{eff} \frac{\partial^2 C(x,t)}{\partial x^2} \quad [6]$$

where $C(x, t)$ is the local concentration in the pore network (kg m^{-3}), and D_{eff} is the diffusion coefficient (m^2 s^{-1}). Equation [6] is solved subject to the initial and boundary conditions

$$C(x,t)|_{t=0} = 0 \qquad 0 < x < l_0 \quad [7]$$

$$C(x,t)|_{x=0} = C_0 \qquad t > 0 \quad [8]$$

$$\left.\frac{\partial C(x,t)}{\partial x}\right|_{x=l_0} = 0 \qquad t > 0 \quad [9]$$

where l_0 is the length of the soil sample (in our case 50 mm). The method of separation of variables (Mathews and Walker, 1970) may be used to obtain an exact solution:

$$\frac{C(x,t)}{C_0} = 1 - \frac{4}{\pi} \sum_{n=0}^{\infty} \frac{1}{2n+1} \exp\left[\frac{-\left(n+\frac{1}{2}\right)^2 \pi^2 D_{eff}}{l_0^2} t\right] \sin\left[\frac{\left(n+\frac{1}{2}\right)\pi x}{l_0}\right] \quad [10]$$

This solution was previously published also by Carslaw and Jaeger (1959, p 96).

Fractal Dimension of Shortest Path

As pointed out by Middlemiss et al. (1980), the fractal dimension D_{mp} alone is not sufficient to describe all fractal objects. A new parameter D_{min} was introduced by Havlin and Nossal (1984) to describe the tortuosity of the fractals. Kimmich et al. (2001) found that for fluid transport in porous media and percolation clusters, D_{min} plays a more important role than D_{mp}. Fractals with nearly identical D_{mp} values can have quite different values of D_{min}. The length of shortest path l_{min} obeys the following relationship (Havlin and Nossal, 1984)

$$l_{\text{min}} \propto r^{D_{\text{min}}} \quad [11]$$

MATERIALS AND METHODS

Binary Images

Binary images of soil thin sections (Fig. 2) were selected from a recent publication by Anderson et al. (2000). The images in their study were obtained from black-and-white photographs of the thin sections. Two images were made from each photograph, one representing the upper half of the thin section and another one the lower half. The location from which each thin section was taken, soil type and other characteristics of the thin sections are described in Anderson et al. (1996). We did not use Soils 1 and 2 from their study because of the poor connectivity of the pore networks, which we found very difficult to simulate (no paths to link the inlet and the outlet). Hence, eight groups of soil thin sections were selected. The images had dimension of 50 by 50 mm. Gray level 1 was used for the solid phase (the white areas of the photographs), while the pore phase of the real soil (the black areas) was represented by gray level 0.

We converted the images from 1000 by 1000 pixels to 2000 by 2000 pixels using Adobe Photoshop (Adobe Systems Inc., San Jose, CA) with the same resolution (96 dpi) as before, while the pore structure was kept as intact as possible. All isolated pores were eliminated from the images. As a result, only the connected pore network was used for the simulations. In this study, we considered only the larger pores (pores > 100 μm), thus implying that the remaining pore space is part of the solid phase.

To separate the effects of structure parameters (ε, D_{mp}, D_{min}, and the porosity of the shortest path ε_{min}) on diffusion, eight original thin sections of Anderson et al. (2000) were processed with the Wintopo (SoftSoft Ltd., Bedfordshire, SG, UK) software package to change the thickness of lines (corresponding to the paths in images or thin sections) while keeping the same air-filled porosity ε for the given topology (Fig. 2). A box-counting technique as described by Anderson et al. (1996) was used to calculate D_{mp} of the pore space. We further used Release 3 of the SuperMap software (SuperMap GIS Technologies Inc., Beijing, China) to calculate the shortest paths between the inlet and outlet of the 2D pore network. There is a group of possible paths that link a given node on the inlet boundary with a certain node on the outlet boundary. Among these paths, the shortest path is that path that provides the shortest distance between two nodes on the inlet and outlet boundary, respectively. Figure 3a shows all shortest paths linking the inlet and the outlet of soil thin section Soil 3b. The value of D_{min} was estimated in a similar fashion as D_{mp}. Parameters of the pore network are listed in Table 1.

Finite Element Method Diffusion Simulations

Diffusion in each of the 2D thin sections was simulated using Eq. [5] subject to Dirichlet conditions ($C = C_0$) at the inlet boundary, and Neuman conditions ($\partial C/\partial n = 0$, where $\partial/\partial n$ is differentation in the direction of the inward normal) at all other boundaries. For the FEM simulations we discretized the domains using approximately 60 000 6-node triangular elements (Fig. 4a, b, c, d) and approximately 160 000 nodes. The actual number of elements and nodes varied with the sample (see Table 1 for details). We used 6-node triangular elements since they were well suited for irregular grid systems. For each thin section we generated an unstructured finite element mesh using automatic triangulation as implemented in ANSYS (Ansys Inc., Canonsburg, PA) software. Figures 4d and 4e show details of the unstructured mesh and nodes for Sample 3b. We used a Jacobi conjugate gradient solver for solution of the FEM matrix equations.

After each simulation, calculated concentrations were displayed using contour maps as shown in Fig. 4f and Fig. 5. The concentrations hence varied longitudinally in the x direction as well as laterally (perpendicular to the direction of the concentration gradient ∇C, i.e., parallel with the inlet) as shown in Fig. 4g for Soil Sample 3b for three values of x (1, 3 and 5 cm). The average concentration along the outlet boundary (x = 5 cm) was calculated by averaging the nodal concentrations along the outlet, thus leading to breakthrough curves (BTCs) such as shown in Fig. 6. Values of D_{eff} were subsequently estimated from these BTCs by fitting the theoretical curve (Eq. [10]) to the data using the Levenberg-Marquardt package of Mathematica (Wolfram Research Inc., Champaign, IL). Calculated D_{eff} values for the eight soil samples, along with

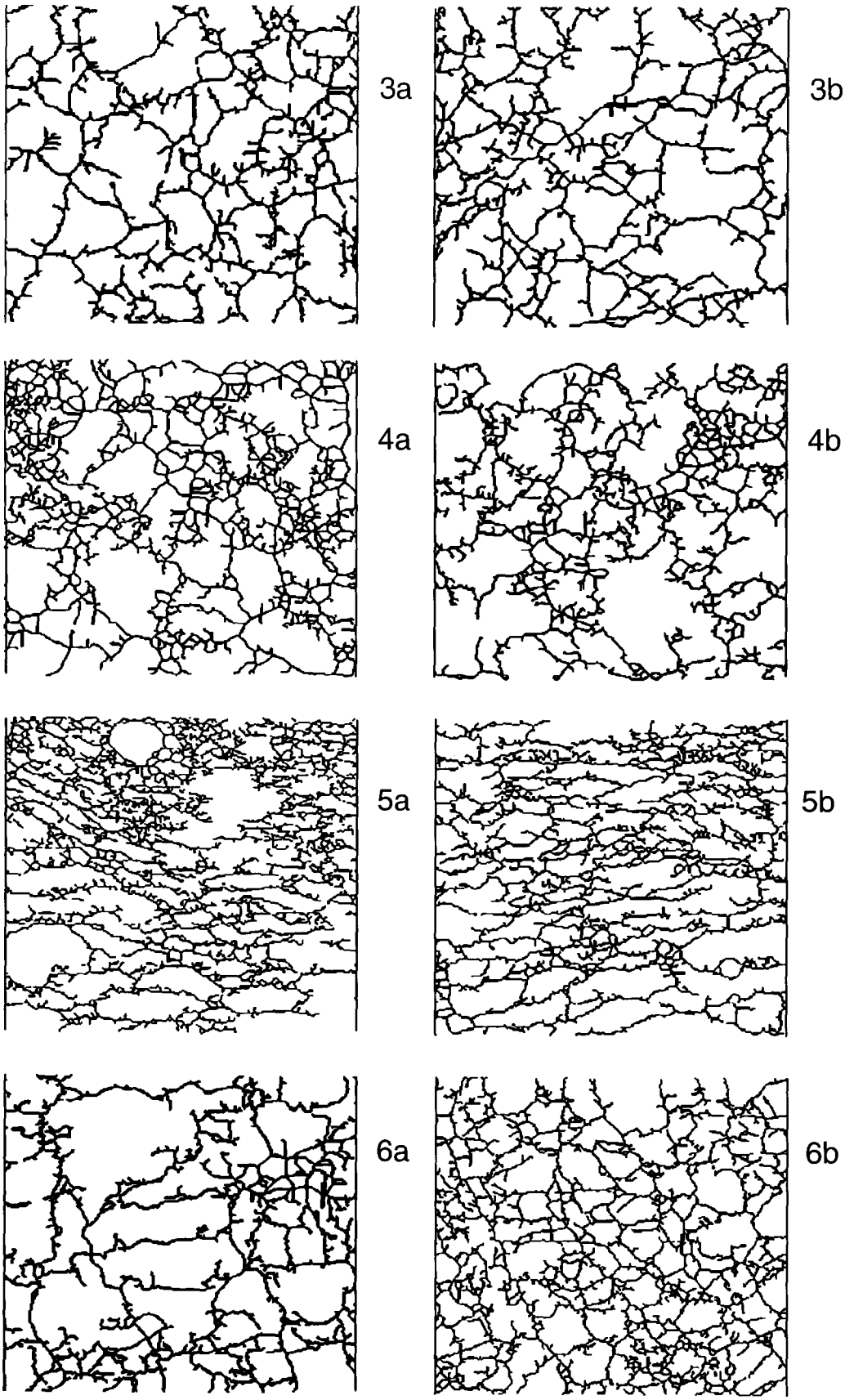

Fig. 2. Binary images of soil thin sections used for the finite element (FEM) solutions (black indicates pores). (a) Top of thin section and (b) bottom of thin section (from Anderson et al., 1996).

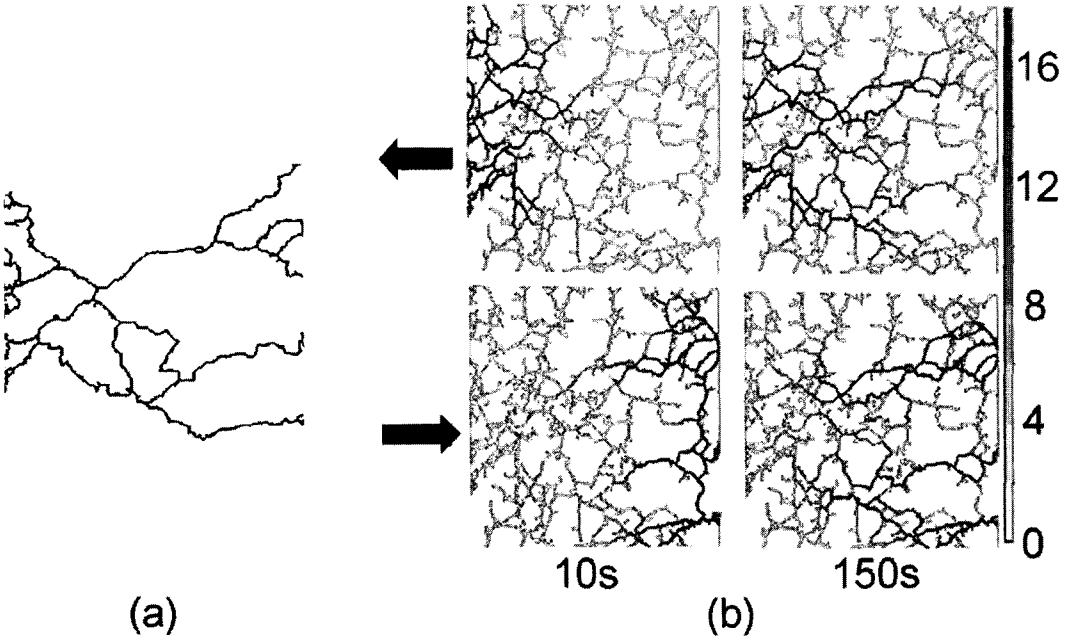

Fig. 3. (a) Plot of the shortest paths for soil thin Section 3b. (b) Diffusive fluxes for soil thin Section 3b for diffusion from left to right (bottom) and right to left (top) after 10 s (left) and 150 s (right).

a number of measured values taken from the literature, are plotted in Fig. 1 as a function of the soil air-filled porosity, ε.

One interesting application of the FEM analysis of the soil thin sections is to study the direction dependency of the diffusion process. This problem was analyzed by reversing the direction of the concentration gradient ∇C, while keeping the initial and other boundary conditions unchanged. For simplicity we selected diffusion in the horizontal (x) direction from left to right and vice versa. Except for reversal of the inlet and outlet boundary conditions, the FEM implementation and discretizations were exactly the same as before.

Verification of Finite Element Simulations

To test the accuracy of our FEM solution of Eq. [5], we simulated diffusion in a square domain with dimensions of 5 × 5 cm, similarly as for the soil thin sections, but now using a regular finite element mesh with nodes that were distributed evenly over the domain (rather than distributed within and along the boundaries of the pore network). D_{eff} was again estimated by fitting Eq. [10] to the BTC. The diffusion coefficient obtained by fitting the FEM simulation using 5000 elements was found to be 1.478×10^{-5} m^2 s^{-1}, which agreed well with the value of 1.500×10^{-5} m^2 s^{-1} used in the calculations (Fig. 6a). Hence, the adopted procedure should give accurate results for the effective diffusion coefficient in the soil thin sections assuming applicability of Fick's law at the pore scale.

Error Analysis of the Finite Element Simulations

To gain further insight in possible errors of the FEM solution, a sensitivity analysis was performed before the simulations with the digitized soil thin sections. We calculated the relative diffusion coefficient ξ of the thin section of Soil 3b using increasingly finer meshes with 17 120, 67 464, and 269 856 elements. Figure 6b shows plots of the BTCs at the outlet. We found that the FEM results for the mesh with 67 464 elements differed at most 3% from results using 269 856 elements. The computation time for the simulations with 67 464 elements (which required approximately 300 time steps) on a Pentium IV personal computer with 1 GB DDR main memory varied between 8 and 12 h per sample. The simulation with 269 856 elements continued for at least 2 d and generated a very large data file of nearly 50GB. As a compromise between less computation time and smaller errors, we hence used approximately 60 000 elements for the simulations on all eight samples.

RESULTS AND DISCUSSION

Comparison of Finite Element Simulations with Current ξ(ε) Models

No unique relationship was found between the relative diffusion coefficient (ξ) and the air-filled porosity (ε). Figure 1a presents published experimental data of

Table 1. Parameter values (ε, Φ, ε_{min}, D_{mp}, D_{min}) and number of elements (N_{elements}) used for the finite element (FEM) simulations of diffusion in soil thin sections. Calculated values of ξ as a function of the direction of ∇C (from right to left, $\xi_>$) and vice versa ($\xi_<$) are also given.

Soil sample	3a	3b	4a	4b	5a	5b	6a	6b	Mean	σ
ε	0.1624	0.1626	0.1623	0.1622	0.1623	0.1624	0.1623	0.1620	0.1623	0.00017
Φ	0.1723	0.1765	0.1650	0.1712	0.1774	0.1782	0.2064	0.1789	0.1782	0.0122
ε_{min}	0.0622	0.0542	0.0685	0.0491	0.0528	0.0654	0.0538	0.0560	0.0578	0.0068
D_{mp}	1.626	1.616	1.881	1.745	1.633	1.704	1.552	1.592	1.668	0.105
D_{min}	1.583	1.579	1.505	1.549	1.461	1.504	1.603	1.509	1.537	0.0494
N_{elements}	70620	67464	77582	55528	74553	57414	63070	69564	66966	7817
$\xi_>$	0.0222	0.0168	0.0210	0.0218	0.0191	0.0193	0.0234	0.0202	0.0205	0.0021
$\xi_<$	0.0135	0.0197	0.0294	0.0164	0.0212	0.0223	0.0124	0.0231	0.0198	0.0056
$\xi_>/\xi_<$ (%)	164.44	85.28	71.43	132.93	90.09	86.54	188.71	87.45	114.91	42.46

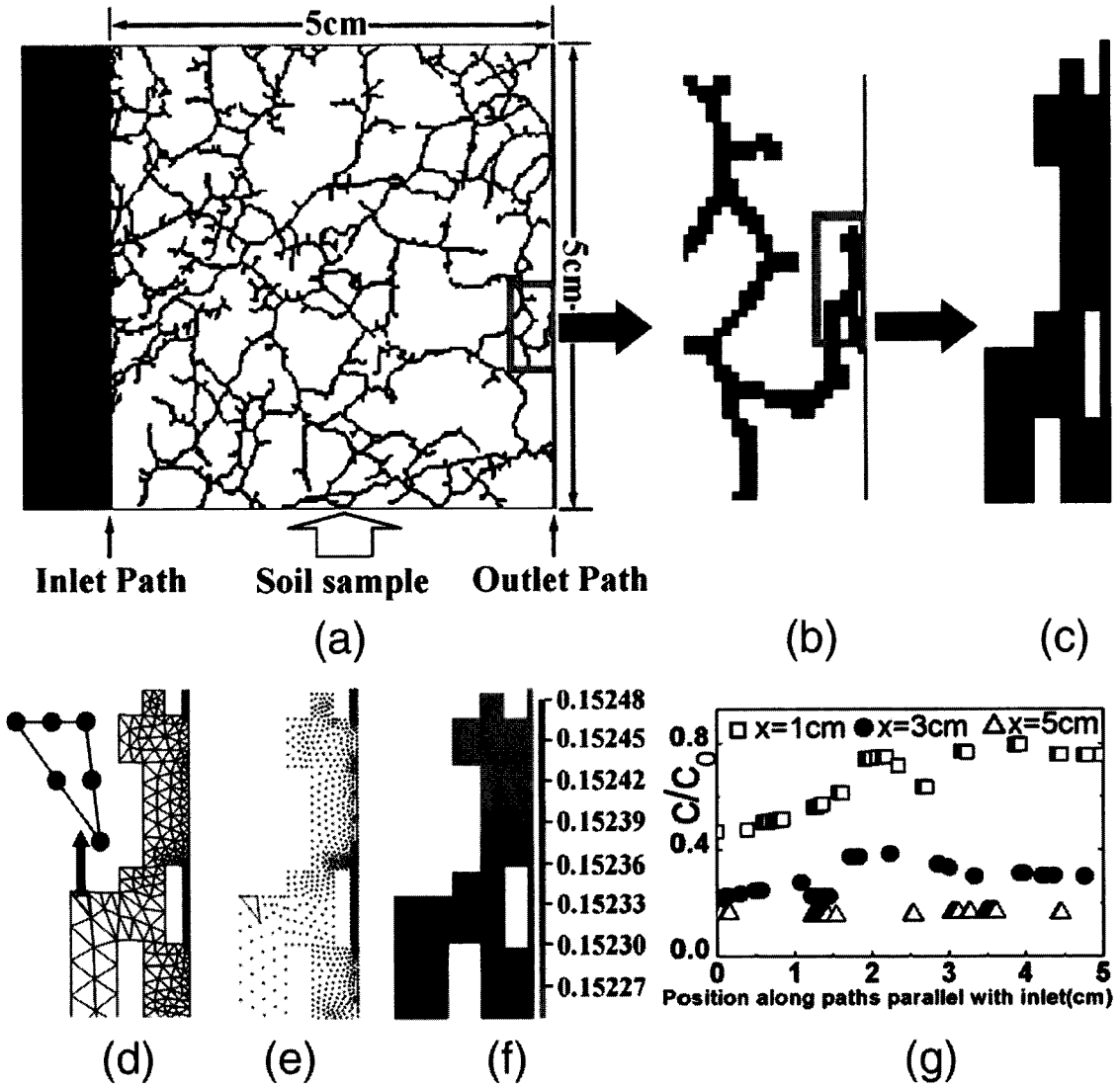

Fig. 4. (a) Schematic of the two-dimensional diffusion simulation system in which diffusion occurs from the dark area on the left of the soil thin section to the right. (b) and (c) represent enlarged parts of the thin section as displayed within the gray lines of (a) and (b). (d) shows the unstructured mesh adopted for the finite element (FEM) simulations, including a typical enlarged 6-node triangular element (indicated by arrow) used in the simulations. (e) shows nodes of the computational mesh. (f) gives a contour plot of the concentration field at time t = 150 s. (g) example of concentration distribution (t = 150 s) along the paths (x = 1, 3, and 5 cm).

$\xi = D_{eff}/D_0$, plots of the commonly used MQ-1 (Millington and Quirk, 1960) and MQ-2 (Millington and Quirk, 1961) models, and ξ values obtained with our FEM simulations of the soil thin sections. The MQ-1 and MQ-2 curves were generated for two different Φ values (0.4 and 0.8), thus bracketing the porosity for a wide range of soil types. Figure 1b is an enlarged part of Fig. 1a with ε between 0.12 and 0.18. To better distinguish between ξ values obtained with opposite concentration gradients in C, we shifted the FEM simulation results in Fig. 1b slightly around $\varepsilon = 0.1623 \pm 0.0002$ (+ for diffusion from left to right, and × for diffusion from right to left). The results in Fig. 1 show that neither the MQ-1 model nor MQ-2 described the $\xi(\varepsilon)$ points obtained with our FEM analysis of the soil thin sections. This agrees with Bruckler et al. (1989) who also found no unique relationship between the porosity and the diffusion coefficient (Fig. 1). Jin and Jury (1996) attributed the fluctuations in ξ between independent experimental studies to the heterogeneous nature of soils.

We note that our FEM simulation results may be subject to three possible errors. First, processing of the original thin sections with the Wintopo (SoftSoft Ltd., Bedfordshire, SG, UK) software to change the thickness of lines could have led to a distortion of the topological network of pores. Also, diffusion in pore systems (experimental data of Fig. 1a) is a 3D process, while our simulations were performed in 2D. Finally, because of the finite resolution of the photographs, digitized thin sections may not include all of the pores, especially the finer pores, which could lead to overly conservative estimates of the connectivity and porosity of a real soil. In view of these possible errors and the fact that only the larger pores were considered in our FEM simulations,

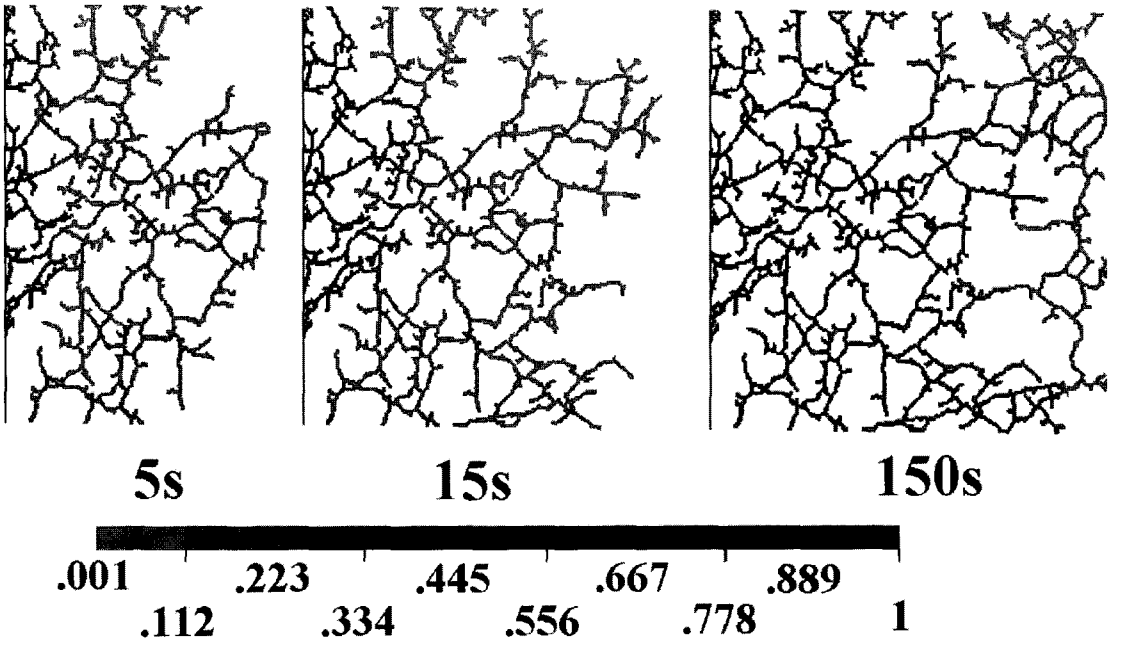

Fig. 5. Contour plots of concentrations obtained with the finite element (FEM) simulations for diffusion in soil thin Section 3b.

the calculated ξ values of the idealized soil systems we studied appear to be well within a realistic range of values (Fig. 1a and 1b). It still remains unclear if our method can be used to obtain realistic estimates of the gaseous diffusion coefficient of actual field soils. We believe that the method is quite promising for estimating the diffusion coefficient of macroporous soils, fractured rock or other dual-porosity media (such as fractured limestone) which have a more distinct division between relatively large pores (the macropores or fractures) and very small, relatively inactive micopores within soil aggregates or within the rock matrix.

Fractal Dimension

After completing the FEM simulations we used the fractal dimension of pores (D_{mp}) to try to establish a scaling relationship for ξ. We were unable to find a universal exponent or unique relationship between ξ and D_{mp}. Because of the poor correlations, these results are not fur-

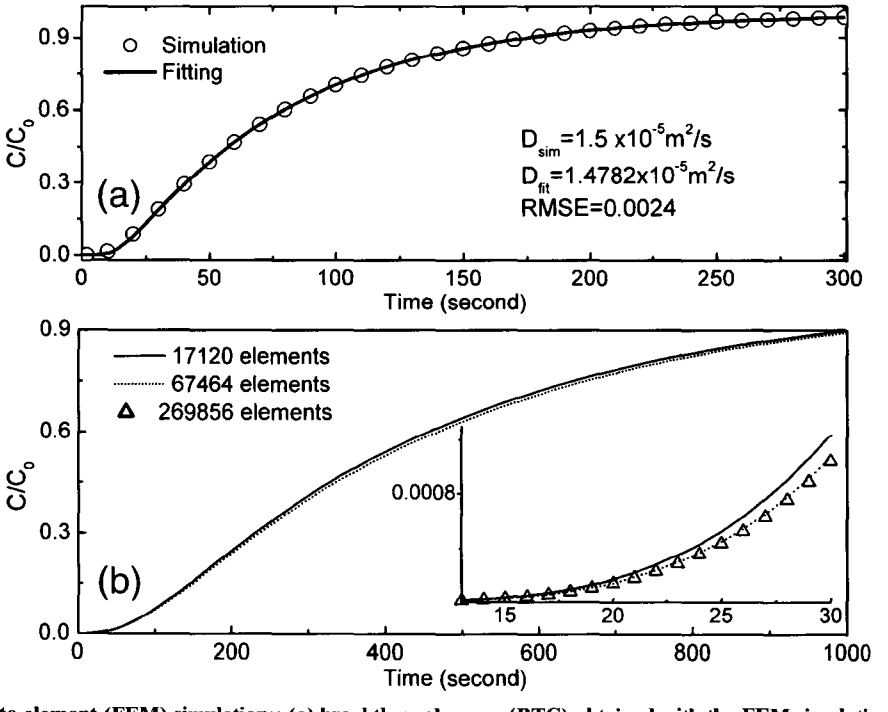

Fig. 6. Results of the finite element (FEM) simulations; (a) breakthrough curve (BTC) obtained with the FEM simulation (C) and corresponding fitted curve (solid line). (b) FEM simulation with different mesh densities for Soil Sample 3b.

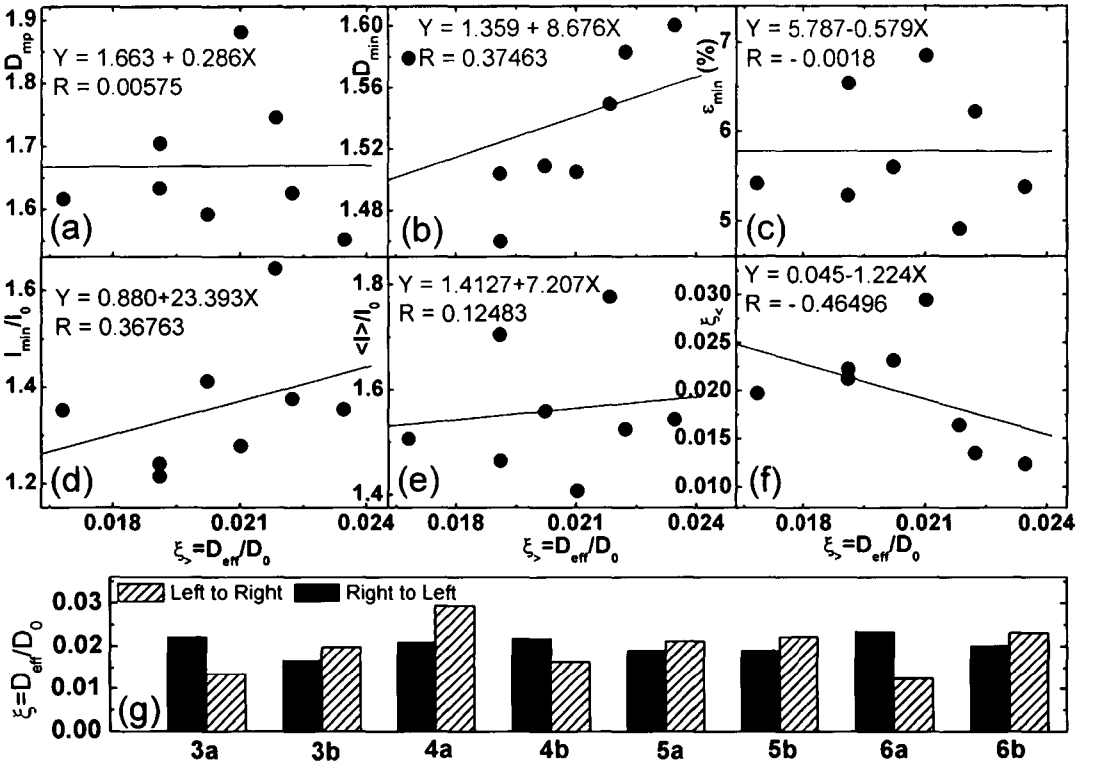

Fig. 7. Relationships between soil structure parameters [(a) D_{mp}, (b) D_{min}, (c) ε_{min}, (d) $\langle l_{min}\rangle/l_0$, (e) $\langle l\rangle/l_0$, (f) $\xi_<$ and $\xi_>$, respectively]. (g) ξ values obtained by fitting the finite element (FEM) simulated breakthrough curve (BTC) (results for diffusion from left to right and right to left).

ther discussed here. As shown for example in Fig. 7a, we found essentially no correlation between ξ and D_{mp} (the correlation coefficient R was only 0.005 75). In other words, for our samples having a relative narrow range of ε values (0.1623 $\pm$ 0.0002), we could not determine which sample had the higher ξ value using only the value of D_{mp}. Our results disagree with the predictive model of Anderson et al. (2000), who obtained the relationship

$$\xi = \varepsilon(r_c)^{[2(1-D_{mp}/d)]/(D_{mp}-2)} \left(\frac{r_c}{r_1}\right)^{-[2(D_{mp}-d)/d + D_{mp}-2]} \quad [12]$$

where d is the spectral dimension, r_c is the characteristic diameter of the image and r_1 the characteristic length.

Fractal dimension is not the only parameter that may affect the diffusion process. The value of D_{min} also plays a potentially important role in the diffusion properties of fractal systems, as indicated by several theoretical studies and Monte-Carlo simulations (e.g., Havlin and Nossal, 1984; Kimmich et al., 2001). For this reason we also closely examined D_{min}. Although we found a positive correlation (R = 0.3746) between D_{min} and ξ in Fig. 7b, the relationship was not strong enough to define a universal relationship using the simulation data. We also studied possible correlations between ξ and the porosity of the shortest path. No or only very weak negative correlations were found between ε_{min} and ξ, as indicated by Fig. 7c.

The Role of the Shortest Diffusion Path

The FEM simulations allowed us to re-examine the physical basis of the tortuosity T, which is considered to be an important parameters affecting flow and transport in porous media. Current definitions of tortuosity are mostly empirical in nature, and do not readily permit direct and independent measurement.

Based on the results of Fig. 3, 7a, 7b, and 7c, we found that for most samples the shortest paths had more effect on ξ as compared with D_{mp} and ε. To be consistent with the popularly used definition of tortuosity, we plotted the average relative length of the shortest paths (i.e., $\langle l_{min}\rangle/l_0$) and the average relative length of all paths (i.e., $\langle l\rangle/l_0$) between the inlet and the outlet versus ξ ($\langle..\rangle$ indicates averaging over all possible values). The correlations are shown in Fig. 7d (R = 0.3676) and Fig. 7e (R = 0.1248), respectively. While some correlation exists between $\langle l_{min}\rangle/l_0$ and ξ, the correlation between $\langle l\rangle/l_0$ and ξ is very weak or essentially nonexistent. Figures 3a, 3b should support this finding in that, as compared with the other paths, the shortest paths will contribute relatively more to the total diffusive flux, which is defined as the total mass of gas moving across a unit area of the pores per unit time. Still, while the shortest paths such as those shown in Fig. 3a are responsible for most of the diffusion flux (Fig. 3b), the influence of the other paths should not be negligible.

In view of the results in Fig. 7, we suggest that for simplicity the tortuosity T is related to the shortest paths by $T = \langle l_{min}\rangle/l_0$. A more accurate definition of T probably should include all other paths along with weighting factors to reflect their contribution to the total diffusive flux. The tortuosity would then be given by

$$T = \frac{\sum_{i=1}^{n} w(l_i) l_i}{l_0} \quad [13]$$

where $w(l_i)$ is the weight of the *ith* path l_i. Unfortunately detailed knowledge about the weights is generally not available.

Because our simulations do not involve any experimental errors, the fluctuations in the simulation results can be attributed only to the pore-space morphology. Still, because of the finite size of the digitized samples (2000 × 2000 pixels for all samples), some errors may have resulted from using a finite domain. The more pores included in the simulation, the more accurate and smooth the result should be.

The results of Fig. 7g indicate that diffusion (from left to right) is greatest for Soil 4a, which has well-connected pores and has a more homogeneous pore-size distribution than the others samples. Soil samples that contain more dead-end pores, such as Sample 6a, should have a lower pore connectivity and relatively smaller ξ value than the others. A close comparison of the structures of the samples with the largest (4a) and smallest (6a) values of ξ, indicates relatively more paths between the inlet and the outlet for 4a as compared with 6a. This should reflect the more homogeneous makeup of the pore network of Sample 4a relative to 6a as shown in Fig. 2.

Directional Dependency of the $\xi(\varepsilon)$ Relationship

In Fig. 1, we plotted a series of ξ values obtained from the FEM simulations on eight samples with opposite directions of the concentration gradient ∇C (+ values indicating diffusion from left to right, and × values for diffusion from right to left). One remarkable finding is the considerable fluctuation in the ratio of the two ξ values (i.e., of $\xi_>/\xi_<$) of samples with approximately the same ε. This can be seen more clearly in Fig. 7g and Table 1. For soil Samples 6a and 3a, ξ changed 89 and 64%, respectively, when the concentration gradient was reversed. For soils 5a and 6b the changes were −10 and −13%, respectively. A closer examination of the pore structures shows that more pores are on the right-hand sides of Samples 6a and 3a. The moderate negative correlation between $\xi_>$ and $\xi_<$ (with $R = -0.46496$) as plotted in Fig. 7f suggests that a larger $\xi_>$ more likely corresponds to a smaller $\xi_<$ for the same sample, which means that the pore-space structure near the outlet dominates the behavior of ξ. The pore distributions along the direction of ∇C cannot be described by ensemble average parameters such as ε, Φ, D_{mp}, and D_{min}, which smooth the information of the heterogeneous pore structure. The strong direction dependency of ξ indicates that no universal exponent seems to exist for ensemble average parameters.

Explanation of the Direction Dependent $\xi(\varepsilon)$ Relationship

The direction dependency of $\xi(\varepsilon)$ is a result of the pore network being inhomogeneous in that more pores are present on one side and less pores on the other side. The diffusion process is then affected by spatial variations in the pore distribution. The total flux across a certain cross-section perpendicular to the direction of ∇C is

$$Q_i = \sum_i j_i \Delta S_i \qquad [14]$$

where $j_i = -D\nabla C_i$ as given earlier by Eq. [3]. Therefore, Q is related to $\sum \Delta S_i$, where ΔS_i is the area of the pores or pathway in the given cross-section. As an example, Fig. 3b shows diffusive fluxes for soil thin Section 3b. If the inlet is connected to many pores, this will lead to a larger diffusion flux than when fewer pores are connected. The value of ξ will then inevitably vary when the direction of ∇C changes continuously. One would expect that the more heterogeneous the pore distribution along the direction of ∇C, the larger the difference will be in ξ between the two opposite directions.

CONCLUSIONS

By means of pore-scale FEM simulations of diffusion in soil thin section images, we investigated the diffusion process in an artificial soil system where all pores smaller than ~100 μm are assumed to be blocked or inactive for gas diffusion. Our study indicates that no simple and unique relationship exists between the diffusion coefficient and porosity for the assumed soil systems of finite size, which agrees with previous experimental findings by Bruckler et al. (1989). Ensemble averaged parameters, such as D_{mp}. D_{min} and ε do not reflect local porosity fluctuations. Therefore, no universal relationship is expected between ξ and D_{mp} or D_{min}. The diffusion process was found to be sensitive to the direction of ∇C, which is related to the pore structure pattern along the direction of the gradient. It is this variation in the distribution that leads to fluctuations in ξ and deviations from the Millington-Quirk (Millington and Quirk, 1960, 1961) models, especially for heterogeneous media. The commonly used tortuosity T is related to the weighted length of the various paths along the direction of the concentration gradient, ∇C.

Based on these results we suggest several recommendations for diffusion experiments. For laboratory experiments, careful soil packing is essential. Heterogeneity in the pore connectivity will lead to uncertainties in ξ. For diffusion studies, especially when using undisturbed field samples, the experiments should be performed in different directions to evaluate the influence of pore-structure heterogeneity. If pores are present whose size is comparable with the sample size, then the value of ξ likely will become very sensitive to the diffusion direction. To minimize uncertainties caused by a heterogeneous pore structure, relatively large samples (i.e., much larger than the mean pore diameter) or compacted soil (which has a more homogeneous pore network with fewer fractures) should be used. If this is not possible, experiments with different ∇C directions should be performed. Variations in ξ as a function of the ∇C direction could be used as a criterion for characterizing soil structure heterogeneity. The larger the difference, the more heterogeneous the pore network is expected to be.

ACKNOWLEDGMENTS

We appreciate the generous efforts of Yadong Liu to provide FEM software package and thank Tusheng Ren for valuable discussions. This work was supported by program for Changjiang Scholars and Innovative Research Team in University (Proj-

ect IRT0412) of P.R. China. The financial support of China National Natural Science Foundation [Grant No. G40201022 (G.L.) and G40401025 (K.H.)] is gratefully acknowledged.

REFERENCES

Alvarez-Ramirez, J., S. Nieves-Mendoza, and J. Gonzalez-Trejo. 1996. Calculation of the effective diffusivity of heterogeneous media using lattice-Boltzmann method. Phys. Rev. E. 53:2298–2303.

Anderson, A.N., A.B. McBratney, and E.A. FitzPatrick. 1996. Soil mass, surface, and spectral dimensions estimated from thin section photographs. Soil Sci. Soc. Am. J. 60:962–969.

Anderson, A.N., J.W. Crawford, and A.B. McBratney. 2000. On diffusion in fractal soil structures. Soil Sci. Soc. Am. J. 64:19–24.

Arah, J.R.M., and B.C. Ball. 1994. A functional model of soil porosity used to interpret measurements of gas diffusion. Eur. J. Soil Sci. 45: 135–144.

Bolvin, H., A. Chambarel, and A. Chanzy. 2004. Three-dimensional numerical modeling of a capacitance probe: Application to measurement interpretation. Soil Sci. Soc. Am. J. 68:440–446.

Brenner, S.C., and L.R. Scott. 1994. The mathematical theory of finite element methods. Springer-Verlag, New York.

Brown, B.D., and D.E. Rolston. 1980. Transport and transformation of methyl bromide in soils. Soil Sci. 130:68–75.

Bruckler, L., B.C. Ball, and P. Renault. 1989. Laboratory estimation of gas diffusion coefficient and effective porosity in soils. Soil Sci. 147:1–10.

Buckingham, E. 1904. Contributions to our knowledge of the aeration of soils. USDA Bur. Soil Bul. 25. U.S. Gov. Print. Office, Washington, DC.

Carslaw, H.S., and J.C. Jaeger. 1959. Conduction of heat in solids. 2nd ed. Oxford Univ. Press, London.

Fick, A.E. 1855. Über diffusion. Annalen der Physike, Leipzig. 94:59–86.

Graham, T. 1850. On the diffusion of liquids. Philos. Trans. R. Soc. 140: 1–46.

Havlin, S., and R. Nossal. 1984. Topological properties of percolation clusters. J. Phys. A 17:L427–L432.

Jin, Y., and W.A. Jury. 1996. Characterizing the dependence of gas diffusion coefficient on soil properties. Soil Sci. Soc. Am. J. 60:66–71.

Karimi, A.A., W.J. Farmer, and M.M. Cliath. 1987. Vapor phase diffusion of benzene in soil. J. Environ. Qual. 16:38–43.

Kimmich, R., A. Klemm, and M. Weber. 2001. Flow, diffusion, and thermal convection in percolation clusters: NMR experiments and numerical FEM/FVM simulations. Magn. Reson. Imaging 19:353–361.

Kruse, C.W., P. Moldrup, and N. Iversen. 1996. Modeling diffusion and reaction in soils: II. Atmospheric methane diffusion and consumption in a forest soil. Soil Sci. 161:355–365.

Marshall, T.J. 1959. The diffusion of gases through porous media. J. Soil Sci. 10:79–82.

Martys, N.S. 1999. Diffusion in partially-saturated porous materials. Mater. Struct. 32:555–562.

Mathews, J., and R.L. Walker. Mathematical methods of physics. 1970. p. 226–239. *In* Partial differentials equations. 2nd ed. W.A. Benjamin, New York.

Middlemiss, K.M., S.G. Whittington, and D.C. Gaunt. 1980. Monte Carlo study of the percolating cluster for the square lattice site problem. J. Phys. A 13:1835–1840.

Millington, R.J., and J.M. Quirk. 1960. Transport in porous media. p. 97–106. *In* F.A. Van Beren et al (ed.) Trans. 7th Int. Congr. Soil Sci., Vol. 1, Madison, WI. 14–24 Aug. 1960. Elsevier, Amsterdam.

Millington, R.J., and J.M. Quirk. 1961. Permeability of porous solids. Trans. Faraday Soc. 57:1200–1207.

Moldrup, P., T. Olesen, T. Yamaguchi, P. Schjønning, and D.E. Rolston. 1999. Modeling diffusion and reaction in soils: IV. The Buckingham-Burdine-Campbell equation for gas diffusivity in undisturbed soil. Soil Sci. 164:542–551.

Moldrup, P., T. Olesen, T. Komatsu, P. Schjønning, and D.E. Rolston. 2001. Tortuosity, diffusivity, and permeability in the soil liquid and gaseous phases. Soil Sci. Soc. Am. J. 65:613–623.

Moldrup, P., S. Yoshikawa, T. Olesen, T. Komatsu, and D.E. Rolston. 2003. Gas diffusivity in undisturbed volcanic ash soils: Test of soil-water-characteristic-based prediction models. Soil Sci. Soc. Am. J. 67:41–51.

Moldrup, P., T. Oleson, S. Yoshikawa, T. Komatsu, and D.E. Rolston. 2004. Three-Porosity model for predicting the gas diffusion coefficient in undisturbed soil. Soil Sci. Soc. Am. J. 68:750–759.

Park, Y.J., J.R. de Dreuzy, K.K. Lee, and B. Berkowitz. 2001. Transport and intersection mixing in random fracture networks with power law length distributions. Water Resour. Res. 37:2493–2501.

Peng, G., H. Xi, C. Duncan, and S. Chou. 1998. Lattice Boltzmann method on irregular meshes. Phys. Rev. E. 58:R4124–R4127.

Penman, H.L. 1940. Gas and vapor movements in the soil. I. The diffusion of vapors through porous solids. J. Agric. Sci. (Cambridge) 30:437–462.

Petersen, L.W., Y.H. El-Farhan, P. Moldrup, D.E. Rolston, and T. Yamaguchi. 1996. Transient diffusion, adsorption, and emission of volatile organic vapors in soils with fluctuating low water contents. J. Environ. Qual. 25:1054–1063.

Rassam, D., J. Simunek, and M.Th. van Genuchten. 2003. Modelling variably-saturated flow with HYDRUS-2D. ND Consult, Brisbane, Australia.

Satoh, S., I. Matsuyama, and K. Susa. 1995. Diffusion of gases in porous silica gel. J. Non-Cryst. Solids 190:206–211.

Steele, D.D., and J.L. Nieber. 1994. Network modeling of diffusion coefficients for porous media: I. Theory and model development. Soil Sci. Soc. Am. J. 58:1337–1345.

Taylor, S.A. 1949. Oxygen diffusion in porous media as a measure of soil aeration. Soil Sci. Soc. Am. Proc. 14:55–61.

Weerts, A.H., D. Kandhai, W. Bouten, and P.M.A. Sloot. 2001. Tortuosity of an unsaturated sandy soil estimated using gas diffusion and bulk soil electrical conductivity: Comparing analogy-based models and lattice-Boltzmann simulations. Soil Sci. Soc. Am. J. 65:1577–1584.

Xu, X., J.L. Niber, and S.C. Gupta. 1992. Compaction effects on the gas diffusion coefficient in soils. Soil Sci. Soc. Am. J. 56:1743–1750.